Steel and Composite Structures, *Vol. 56, No. 5 (2025) 405-417*
https://doi.org/10.12989/scs.2025.56.5.405

Experimental validation of the transmission tower designed using load and resistance factor design method in South Korea

Whi Seok Han[1a], Pyounghwa Kim[1b], Jeong Hun Kim[2c], Hunhee Cho[1d] and Seungjun Kim*[1]

[1]*School of Civil, Environmental, and Architectural Engineering, Korea University, Seoul, Korea*
[2]*Next Generation Transmission & Substation Lab., KEPCO Research Institute, Daejeon, Korea*

(Received May 15, 2025, Revised June 27, 2025, Accepted July 7, 2025)

Abstract. This study proposes and validates a load and resistance factor design (LRFD)-based approach for 345 kV transmission towers in South Korea. A new tower was designed following LRFD principles and compared to an existing tower developed using the conventional allowable stress design (ASD) method. The LRFD-based design achieved an approximate 11% reduction in structural weight by optimizing member sizing. Structural vulnerabilities and nonlinear failure behaviors under critical load combinations were first identified through finite element analysis and subsequently verified via full-scale load testing. The experimental program assessed structural performance under four major LRFD load combinations and benchmarked the results against those derived from ASD conditions. Additionally, the ultimate strength and failure characteristics were investigated under extreme wind loading with all conductors intact. Despite the reduced member sizes, the LRFD-designed tower satisfied all load-bearing requirements. The failure test, conducted by incrementally increasing the applied load, revealed a buckling failure at 135% of the design load, closely aligning with the nonlinear analysis predictions. These findings confirm that the proposed LRFD-based approach ensures both structural reliability and material efficiency, offering a valuable reference for the optimization and enhancement of future transmission tower designs.

Keywords: failure analysis; full-scale test; LRFD-based design; nonlinear analysis; transmission tower

1. Introduction

Transmission towers are an integral part of modern infrastructure, as they ensure a stable and sustainable supply of electricity to meet contemporary societal demands. Compared with other fundamental structural systems, the transmission tower–conductor system is highly susceptible to environmental hazards, such as extreme winds, icing, and earthquakes, owing to its considerable height and inherent flexibility. Consequently, the system exhibited pronounced nonlinear structural behavior.

However, in South Korea, transmission towers have traditionally been designed using simplified approaches owing to the structural complexity involved, in accordance with the DS-1111 guidelines of the Korea Electric Power Corporation (KEPCO). The simplified design approach referenced here involves applying an "equivalent wind load that assumes a uniform wind pressure distribution along the entire height of the transmission tower during load calculations. For member design, conventional methodology defines member failure as the yielding of material and limits the member stress to within the allowable stress, which is calculated by dividing the yield strength of the material by a prescribed safety factor.

However, there are several limitations to the traditional design approach based on elastic limits. First, it does not accurately capture the potential vulnerabilities of a structure, making it difficult to determine the maximum load-bearing capacity owing to the lack of a failure mechanism. Second, exceeding the yield stress in an individual member does not necessarily imply the collapse of the entire structural system.

Therefore, over the past few decades, extensive research has been conducted using various methods, including substructure testing, numerical simulations, and full-scale testing, to investigate the failure mechanisms and maximum load-bearing capacity of lattice transmission towers constructed with angle-section members in more detail.

Numerical-simulation-based studies excel at analyzing the progressive failure mechanisms of transmission towers, offering cost efficiency and repeatability that enable the exploration of various failure scenarios. These include the finite particle method proposed by Yu *et al*. (2011), geometric imperfection method by Wang *et al*. (2021), buckling and softening failure method proposed by Zheng *et al*. (2017), and Tian-Ma-Qu constitutive model developed by Tian *et al*. (2023). Additionally, Kim *et al*. (2010) investigated the ultimate strength and failure behavior of local components using a partially scaled model, providing a direct approach for validating the numerical analysis results and partially ensuring the safety and reliability of transmission towers.

Various localized regions of transmission towers were

*Corresponding author, Ph.D. Associate Professor
E-mail: rocksmell@korea.ac.kr
[a]Ph.D. Student
[b]Ph.D. Research Professor
[c]Ph.D. Senior Researcher
[d]Ph.D. Professor

ISSN: 1229-9367 (Print), 1598-6233 (Online)

experimentally investigated. These include physical tests of local models, such as tubular joints (Deng *et al*. 2017, Tian *et al*. 2020a), cross arms (Zhang *et al*. 2022), leg members (Deng *et al*. 2018, Li *et al*. 2017), and L-shaped joints (Ma *et al*. 2021). The most effective method for identifying the vulnerabilities and failure mechanisms of transmission towers is full-scale experimental verification (Rao *et al*. 2012). Tian *et al*. (2020b) and Fu *et al*. (2019) conducted full-scale tests to investigate the failure mechanisms of transmission towers under various loading scenarios. Kim *et al*. (2023, 2025a, 2025b, 2025c, 2025d, 2025e, 2025f, 2025g) and Han *et al*. (2025) explored the ultimate load-carrying capacities of simplified transmission tower designs using member optimization techniques. In addition, Darestani *et al*. (2019), Song *et al*. (2022), and Roman *et al*. (2024) advanced the collapse simulation of transmission towers by incorporating the effects of bolt slippage.

The overarching goal of this study was to enhance the design efficiency of transmission towers by identifying their failure mechanisms and structurally vulnerable locations. A recurring theme in these studies includes the necessity of considering the ultimate strength beyond the elastic limit, thereby advocating for a more rational design approach that accounts for both elastic behavior and inelastic strength capacity. Despite significant advancements in transmission tower research, direct comparative studies between the allowable stress design (ASD) and load and resistance factor design (LRFD) methodologies are limited. This gap highlights the need for a study that evaluates the differences in structural performance, failure mechanisms, and load-bearing capacities under these two distinct design approaches.

Therefore, this study designs a 345 kV lattice transmission tower using member strength equations and investigates its failure behavior and ultimate strength through nonlinear analysis and full-scale testing. The analysis results indicated that the failure behavior of the transmission tower progressed gradually, primarily owing to the buckling of the leg members or flexural failure caused by the partial yielding of the compression members.

Sections 4-5 present full-scale tests conducted to validate these findings. Strain gauges were attached to the structurally vulnerable members and those expected to experience critical stress under various load combinations. The tests evaluated the load-carrying capacity under different loading scenarios and conducted failure tests under governing design load cases. A comparison between the experimental and analytical results demonstrated that the material nonlinear analysis predicted the actual tower behavior more accurately. The consistency between the experimental and analytical results validates the member strength equations that consider inelastic strength, reinforcing their applicability. Therefore, this study aims to integrate the validated member-strength equations into transmission tower design standards to ensure a more rational and reliability-based structural design framework.

2. Comparative of design code

In South Korea, transmission towers constructed in accordance with DS-1111 are designed using the ASD method, in which member stresses are limited to within the allowable stress range (DS-1111. 2012, Kim *et al*. 2025c). The ASD approach defines member failure as the yielding of material and evaluates the allowable stress by applying a uniform safety factor of 1.5. However, since the 1970s, the design of many steel structures has shifted toward the LRFD method, which is based on the reliability theory and evaluates member strength based on ultimate limit states. Accordingly, South Korea is currently seeking to update its transmission tower design code to adopt the LRFD approach, with full-scale testing employed to validate the new framework.

The LRFD method is a reliability-based approach that accounts for uncertainties in both loads and resistances by targeting a specific failure probability. It incorporates load factors that reflect the recurrence period and variability of environmental loads, particularly wind loads, as a function of tower height as well as resistance factors based on the different failure modes of the structural members. This study focuses on analyzing the structural behavior of transmission towers using wind loads and member strength equations that apply height-dependent loads and resistance factors derived through reliability analysis. The member stress equations currently used in tower design and the proposed updated member strength equations are presented in Sections 2.1 and 2.2, respectively.

2.1 Previous design code

The design buckling stress equations currently used for transmission towers in South Korea are presented in Eqs. (1)- (2).

When $0 < \lambda_k < \lambda$,

$$\sigma_{ka} = \sigma_{kao} - k_1\left(\frac{\lambda_k}{100}\right) - k_2\left(\frac{\lambda_k}{100}\right)^2 \tag{1}$$

When $\lambda \leq \lambda_k$

$$\sigma_{ka} = \frac{950}{\left(\frac{\lambda_k}{100}\right)^2} \tag{2}$$

where $\lambda_k = L_k/r$ is the effective slenderness ratio, L_k is the effective buckling length, and r is the radius of gyration (mm). σ_{ka} denotes the allowable buckling stress, and σ_{ka0} represents the allowable buckling stress when $\lambda_k = 0$. Coefficients k_1, k_2 are parameters determined by the cross-sectional shape and material properties of the member.

2.2 LRFD design code

The buckling stress equations for the compression members currently being developed by the KEPCO Research Institute are presented in Eqs. (3)-(4).

When $\frac{KL}{r} \leq 4.71\sqrt{\frac{E}{F_y}}$ or $\frac{F_y}{F_e} \leq 2.25$

Table 1 Mechanical properties of wire

Description	Conductor	Shield Wire
Type	ACSR-480	AWS, OPGW
Cross-section area (mm^2)	517.34	182.80
Outside diameter (mm)	29.61	17.50
Weight per unit length (N/m)	15.67	8.28
Maximum allowable tension (kN)	41.65	31.36
Span length (m)	450.0	
Vertical length (m)	800.0	
Line angle (°)	30.0	

$$F_{cr} = \left[0.658^{\frac{F_y}{F_e}}\right] F_y \tag{3}$$

When $\frac{KL}{r} > 4.71\sqrt{\frac{E}{F_y}}$ or $\frac{F_y}{F_e} > 2.25$

$$F_{cr} = 0.877 F_e \tag{4}$$

where F_{cr} denotes the elastic buckling stress, F_y is the yield strength, E is the elastic modulus of steel, K is the effective length factor, L is the unbraced length of the member with respect to lateral buckling, and r is the radius of gyration about the buckling axis. A strength reduction factor ϕ_c of 0.9 was applied. In addition to the member strength equations, environmental loads influenced by climate change were also considered. Using data provided by the Korea Meteorological Administration, wind speed records spanning 60 years (from 1960 to 2020) were extracted to determine the basic design wind speed that accounts for rapidly changing wind load conditions (Kwon *et al*. 2024). Furthermore, wind load estimation equations that reflect surface roughness and height distribution were applied by KBC (2016).

2.3 Comparative transmission tower corresponding design code

To compare transmission towers based on different design codes, a new 345 kV transmission tower was designed and constructed using the LRFD method under the same design conditions as an existing 345 kV tower currently in operation. The load-bearing capacity and ultimate strength of the newly designed tower were then evaluated and compared with those of an existing tower.

Table 1 lists the design and environmental conditions of transmission towers. The transmission tower has a span length of 450 m and a vertical length of 800 m, with a designed horizontal conductor angle of 30°. The conductors used were ASCR-480, whereas the shield wires included AWS and OPGW. The existing 345 kV transmission tower is shown in Fig. 1. The tower had a height of 65.2 m and base width of 13.3 m × 13.3 m. The main structural members vary in height and include sections L120 × 8,

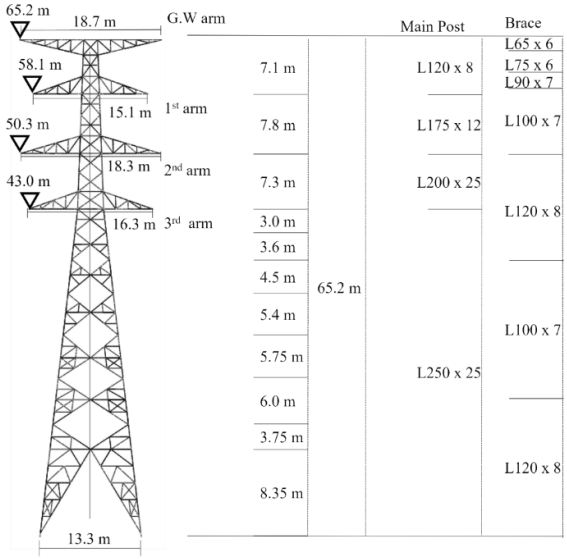

Fig. 1 Structural geometry of the ASD-based transmission tower design

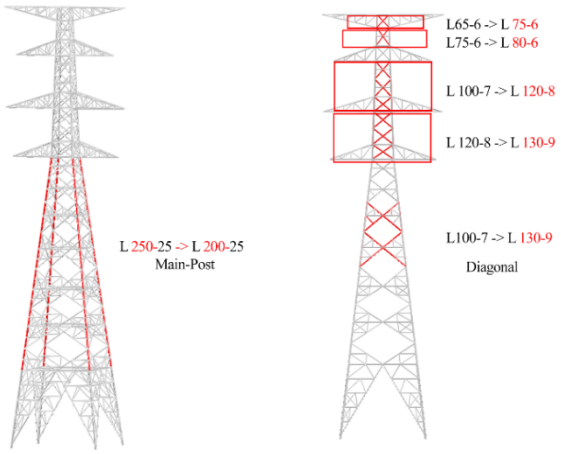

Fig. 2 Optimized geometry in the LRFD-designed transmission tower

L175 × 12, L200 × 25, and L250 × 25. Diagonal members ranged from L65 × 6 to L120 × 8 sections.

The transmission tower, designed using the LRFD approach, adopted the design wind speed based on the wind data for Region III. Based on this, both the wind and conductor loads were evaluated to achieve an optimized structural design (Kwon *et al*. 2024). The differences in the structural members between the existing and newly designed transmission towers are shown in Fig. 2. The material properties of the angled sections are listed in Table 2. The members conformed to Korean Steel Standard KS D 3503. According to KS D 3503, members with dimensions of L 90 × 90 × 6 or smaller have a minimum yield strength of 275 MPa and tensile strength of 410 MPa, whereas members with dimensions of L 90 × 90 × 7 or larger have a minimum yield strength of 410 MPa and tensile strength of 540 MPa.

Notably, the cross section of the primary members from the lower section of the 3rd arm to the upper leg section

Table 2 Mechanical properties of angle member

Type	Section dimension	Yield strength (MPa)	Ultimate strength (MPa)	Elongation (%)
Main post	L 120 × 120 × 8	410	540	14
	L 175 × 175 × 12	410	540	14
	L 200 × 200 × 25	410	540	17
Diagonal	L 75 × 75 × 6	275	410	14
	L 80 × 80 × 6	275	410	14
	L 90 × 90 × 7	410	540	14
	L 100 × 100 × 7	410	540	14
	L 120 × 120 × 8	410	540	14
	L 130 × 130 × 9	410	540	14

could be reduced from L250 × 25 to L200 × 25. However, the diagonal members between the G.W arm and the 3rd arm required an upgrade to a higher section. Owing to the modified cross-sectional design, the weight of the transmission tower was reduced from 53.19 tons to 47.29 tons, representing a decrease of approximately 11.08%.

3. Structural behavior through FEM

3.1 Identification of governing design loads through static analysis

The primary load combinations for the transmission tower designed using the LRFD method are listed in Table 3. The key load combinations included extreme wind conditions, wire failure conditions, and construction conditions, specifically the wire-not-installed condition. Additionally, the load caused by icing was considered for each condition. The static analysis results of the main members at different heights based on the primary load combinations applied to the LRFD-designed transmission tower are shown in Fig. 3.

where f_n represents the nominal strength of the member and f denotes the stress in the member obtained from the analysis. Based on the stress results for each load combination, the governing load for the primary design was the LC1 all-wire-intact load combination, which controlled all the main members from the lower arm to the leg section. However, in the load combinations associated with the non-installed condition (LC8, LC9, and LC10), the stresses were dominant in the lower sections of the main members of each conductor arm. Linear, buckling, and nonlinear analyses were conducted using Abaqus 2023. Structural members were modeled as beam elements with six degrees of freedom. All member connections were assumed to be rigid, simulating the behavior of conventional multi-bolted joints. To more accurately capture structural deformations, each

main post segment was discretized into 10 beam elements, while horizontal and bracing members were modeled with 5 elements each. Fixed boundary conditions were applied at the ends of the bottom leg members to simulate full restraint.

Table 3 Load combinations of LRFD design

No	Load Case	Description	No.	Load Case	Description
1	All wire intact	90° extreme wind	10	CD3 Not Installed	Third wire not installed
2	All wire intact 60°	60° extreme wind	11	One Side Not Installed	Conductors not installed on one entire side of the four arms
3	G.W. Broken	Broken ground wire (shield wire)	12	Normal wind	Normal wind condition
4	CD1 Broken	Broken first wire	13	All wire intact (Low)	90° wind with icing load
5	CD2 Broken	Broken second wire	14	All wire intact_60° (Low)	60° wind with icing load
6	CD3 Broken	Broken third wire	15	G.W. Broken (Low)	Broken ground wire with icing load
7	G.W. Not Installed	Ground wire not installed	16	CD1 Broken (Low)	Broken first wire with icing load
8	CD1 Not Installed	First wire not installed	17	CD2 Broken (Low)	Broken second wire with icing load
9	CD2 Not Installed	Second wire not installed	18	CD3 Broken (Low)	Broken third wire with icing load

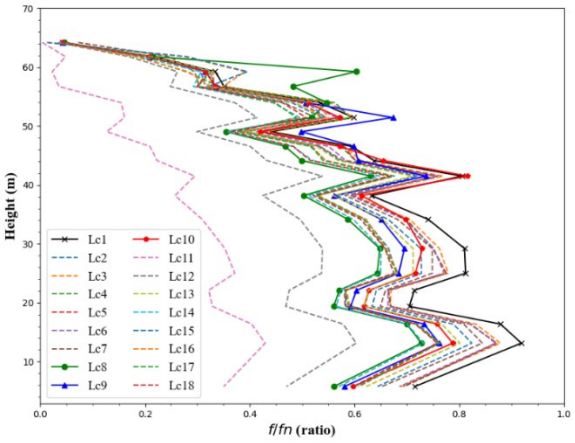

Fig. 3 Static Stress for each load combinations

For the buckling analysis, an eigenvalue analysis was performed using the subspace iteration method. For the nonlinear analysis, an incremental and iterative procedure based on the arc-length method was employed to capture the ultimate behavior, accounting for both geometric and material nonlinearities.

3.2 Identification of structural vulnerabilities using linear buckling behavior

Following the linear analysis, linear buckling analysis was conducted to identify the geometrically vulnerable

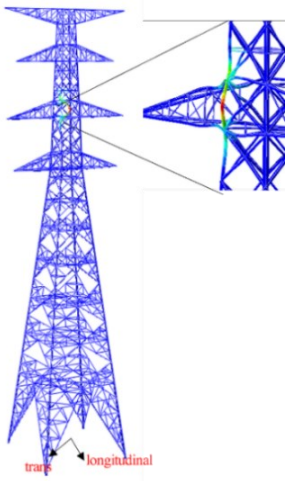

Fig. 4 First Buckling mode at LC1

locations of the structure. The results of the linear buckling analysis, as shown in Fig. 4, indicate that the compression section of the CD2 arm's main member is the most geometrically vulnerable location. At this point, the eigen mode and eigenvalue for LC1 were the lowest, with an eigenvalue of 2.23. Subsequently, a material-geometric nonlinear analysis was performed to evaluate the ultimate strength and failure behavior of the newly designed transmission tower. An elastic-perfectly-plastic material model was applied to conservatively assess the strain behavior in the post-elastic region. To ensure a conservative assessment, the effect of residual stress in members was considered through the LRFD member strength equations (Eqs. (3) and (4)), although it was not explicitly modeled in the numerical analysis. To account for geometric nonlinearity, the mode shape obtained from the linear buckling analysis was adopted as the initial imperfection. An imperfection magnitude of L/500 was applied along this mode shape and incorporated into the subsequent nonlinear finite element analysis. (AISC 2022, Eurocode 3. 2023).

3.3 Identification of ultimate strength through nonlinear behavior

The failure mode of the structure under the LC1 – All-wire-intact load combination is illustrated in Fig. 5, where the failure behavior is represented using the load proportional factor (LPF), which indicates the ratio of the applied load to the design load. Structural failure was initiated when the main members of the tower reached their material yield strengths. Initially, at LPF = 1.05, partial yielding occurred in the compression section of the midbody members, leading to localized plastic deformation. Before the entire cross-section develops into a plastic hinge, load redistribution occurs, causing subsequent yielding in the other structural members. At LPF = 1.07 and LPF = 1.10, partial yielding was observed in the upper leg main members and lower main members of the CD3 arm, respectively. Because multiple locations of the structure resisted the applied load, the tower ultimately reached its ultimate load-bearing capacity at LPF = 1.25, where multiple plastic hinges were formed, leading to structural collapse.

4. Full-scale test

4.1 Experimental Setup through structural behavior

Strain gauges were installed at 42 critical locations to verify the load-bearing capacity of the transmission tower members relative to their design strengths, as shown in Fig. 6. These locations were selected based on static analysis, which identified members experiencing the highest stress; buckling analysis, which determined geometrically vulnerable members and nonlinear analysis, which identified failure initiation points. Specifically, seven strain gauges were installed on the inner and outer surfaces of the L-section members at S9, the location of the highest stress from the linear analysis; at S4, the geometrically vulnerable member identified in the buckling analysis; and at S7, the first failure initiation point from nonlinear analysis, seven strain gauges were installed on both the inner and outer surfaces of the L-section members. At the other selected locations, three strain gauges were attached per section to effectively capture the strain variations.

During the transmission tower testing, six stations were used to measure the lateral and longitudinal displacements of the structure. For further analysis, three unmanned aerial vehicles (UAVs) were deployed to capture aerial footage, and ground-based video recordings were conducted to comprehensively document the structural behavior, as shown in Fig. 7.

4.2 Description of tower

Fig. 8 shows a full-scale test specimen. The test specimens were loaded using two longitudinal reaction towers and one transverse reaction tower. The magnitudes of the applied loads for each test case are listed in Table 4. V, T, and L represent the vertical, transverse, and longitudinal directions, respectively. G denotes the ground wire arm, and C1, C2, and C3 correspond to CD1-arm, CD2-arm, and CD3-arm, respectively. H1 to H4 represent the equivalent wind loads applied to each arm and half of the panel sections between the arms, respectively. Similarly, H5–H7 represent the equivalent wind loads applied to the body panel sections and were applied horizontally.

4.3 Process of test

To validate the key stresses within the members and the design criteria derived from the LRFD method, 10 load combinations were selected for the full-scale load test, as listed in Table 5. Cases 1–9 were used to assess the load-bearing capacities of the structures. These tests followed IEC-60526 (2021) and applied test loads of up to 100% of the specified test loads without including load factors. For Case 10, the ultimate strength of the structure was evaluated by sequentially applying 50%, 75%, 90%, 95%, and 100% factored design loads. After confirming the load-bearing

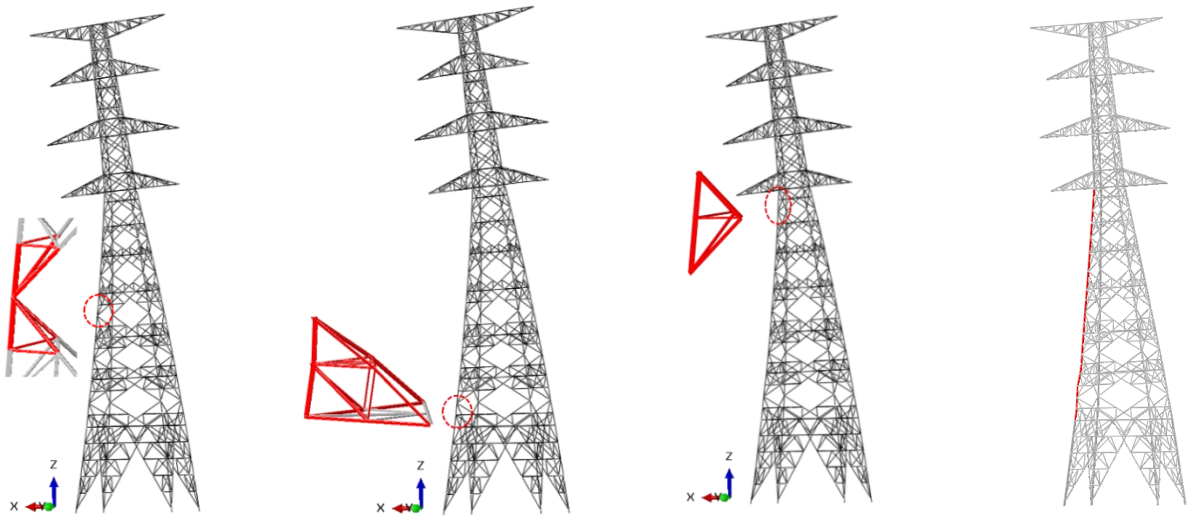

LPF: 1.05 LPF: 1.07 LPF: 1.10 LPF: 1.25

Fig. 5 Collapse process of the transmission tower predicted by FEM at LC1

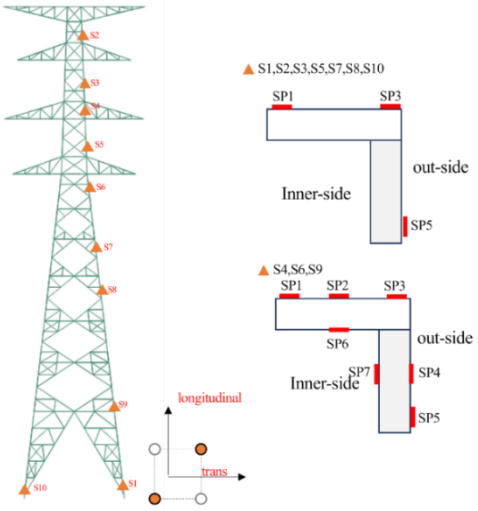

Fig. 6 Measurement points for strain

(a) (b)

Fig. 7 Experimental estimation of structural response using (a) strain gages and (b) UAV-based displacement measurement

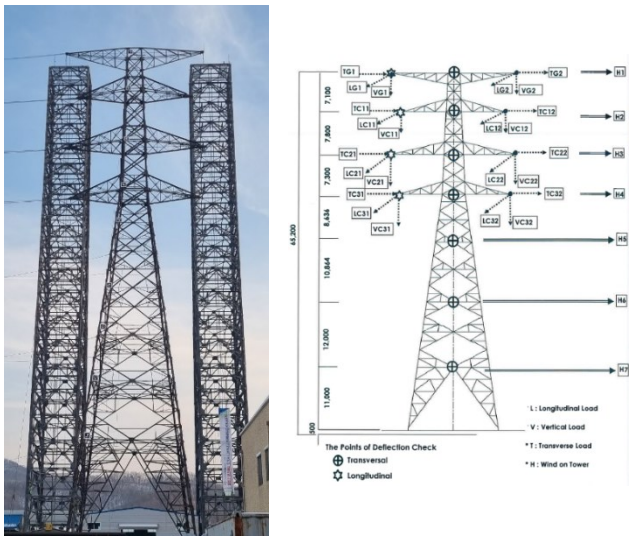

Fig. 8 Overview of full-scale transmission tower and experimental setup

performance at 100%, the load gradually increased in 5% increments until the structures failed.

Case 1 represents a normal wind condition, where the applied wind load corresponds to a design wind speed of 20 m/s. In Cases 2–10, the applied design wind speed was 114 m/s. From Cases 2 to 9, each test was organized into sets of two cases to compare the member stresses under ASD loads and LRFD loads. This setup allows us to directly evaluate the differences in the stress distribution between the two design methodologies.

5. Experimental results and discussion

5.1 Load bearing capacity test

Figs. 9-16 compare the strain responses obtained from the experimental tests and FEM analyses under various load

Table 4 Applied load magnitudes for each loading sequence

Load case		Loading magnitude (kN)									
		LC1	LC2	LC3	LC4	LC5	LC6	LC7	LC8	LC9	LC10
		LRFD	ASD	LRFD	ASD	LRFD	ASD	LRFD	ASD	LRFD	LRFD
Vertical load	VG1	9.2	5.6	5.6	9.2	9.2	9.2	9.2	12.3	12.3	9.2
	VG2	9.2	9.2	9.2	9.2	9.2	0.0	0.0	12.3	12.3	9.2
	VC11	65.3	65.3	65.3	65.3	65.3	65.3	65.3	84.3	84.3	65.3
	VC12	65.3	65.3	65.3	65.3	65.3	0.0	0.0	84.3	84.3	65.3
	VC21	65.3	65.3	65.3	52.8	52.8	65.3	65.3	84.3	84.3	65.3
	VC22	65.3	65.3	65.3	65.3	65.3	0.0	0.0	84.3	84.3	65.3
	VC31	65.3	65.3	65.3	65.3	65.3	65.3	65.3	84.3	84.3	65.3
	VC32	65.3	65.3	65.3	65.3	65.3	0.0	0.0	84.3	84.3	65.3
Transverse load	TG1	22.3	14.0	14.6	24.6	29.2	28.0	29.2	24.6	27.7	33.9
	TG2	22.3	24.6	29.2	24.6	29.2	0.0	0.0	24.6	27.7	33.9
	TC11	102.2	133.2	147.5	133.2	147.5	133.2	147.5	118.9	130.9	175.9
	TC12	102.2	133.2	147.5	133.2	147.5	0.0	0.0	118.9	130.9	175.9
	TC21	101.7	133.2	146.4	100.8	110.9	133.2	146.4	118.9	129.8	174.2
	TC22	101.7	133.2	146.4	133.2	146.4	0.0	0.0	118.9	129.8	174.2
	TC31	100.6	133.2	144.9	133.2	144.9	133.2	144.9	118.9	128.7	172.0
	TC32	100.6	133.2	144.9	133.2	144.9	0.0	0.0	118.9	128.7	172.0
	H1	5.0	5.0	5.0	5.0	5.0	5.0	5.0	2.5	2.5	5.0
	H2	8.1	8.1	8.1	8.1	8.1	8.1	8.1	4.1	4.1	8.1
	H3	9.1	9.1	9.1	9.1	9.1	9.1	9.1	4.6	4.6	9.1
	H4	10.9	10.9	10.9	10.9	10.9	10.9	10.9	5.5	5.5	10.9
	H5	7.1	7.1	7.1	7.1	7.1	7.1	7.1	3.5	3.5	7.1
	H6	11.7	11.7	11.7	11.7	11.7	11.7	11.7	5.9	5.9	11.7
	H7	21.3	21.3	21.3	21.3	21.3	21.3	21.3	10.7	10.7	21.3
	LG1	3.1	31.4	31.4	0	0	3.1	3.1	3.2	3.2	3.1
	LG2	3.1	0	0	0	0	0	0	3.2	3.2	3.1
	LC11	16.7	0	0	0	0	16.7	16.7	16.7	16.7	16.7
	LC12	16.7	0	0	0	0	0	0	16.7	16.7	16.7
	LC21	16.7	0	0	83.3	83.3	16.7	16.7	16.7	16.7	16.7
	LC22	16.7	0	0	0	0	0	0	16.7	16.7	16.7
	LC31	16.7	0	0	0	0	16.7	16.7	16.7	16.7	16.7
	LC32	16.7	0	0	0	0	0	0	16.7	16.7	16.7

combinations (LC2–LC9). Although the strain was measured at numerous locations, this study focused on key measurement points (S4, S7, and S9), as discussed in Section 4.1. The x-axis represents the loading level (%), and the y-axis represents the strain (μm/m). Negative strain values were observed because the members were under compression.

A load test corresponding to LC1, which simulates normal wind conditions, was performed to evaluate the stress behavior of the transmission tower under typical service conditions; however, the results were excluded from this study because they were beyond the primary scope. Furthermore, the LC1 load case itself was utilized to apply preliminary low-level loading to eliminate the potential bolt slippage effects that have been reported in previous studies (Tian *et al*. 2020b, Fu *et al*. 2019, Gao *et al*. 2022)

In the test results for LC2 to LC9—load combinations used to verify the structural capacity of the transmission tower—the measured strains did not exceed the theoretical yield strain of 1950 μm/m (σ_y/E) calculated using simple mechanics. Moreover, no residual plastic strain was observed in any of the strain gauges after unloading. This confirms that the member stresses remained within the elastic range and verifies the structural integrity of the tower.

Furthermore, the strain responses observed in both the experiment and FEM analysis showed similar trends. Across all cases, including the severe C2-Broken condition shown in Figs. 11 and 12, the results at point S4 were consistent between the test and simulation. However, as

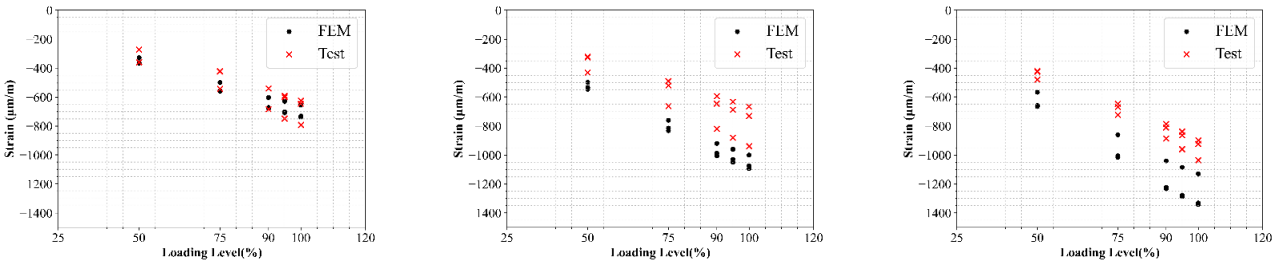

(a) Position S4 (b) Position S7 (c) Position S9

Fig. 9 Comparison of strain responses between the test and FEM results under "G.W Broken" (ASD)

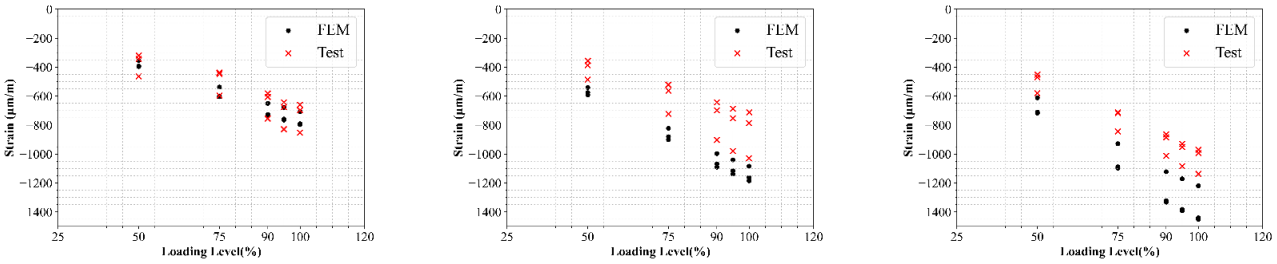

(a) Position S4 (b) Position S7 (c) Position S9

Fig. 10 Comparison of strain responses between the test and FEM results under G.W Broken (LRFD)

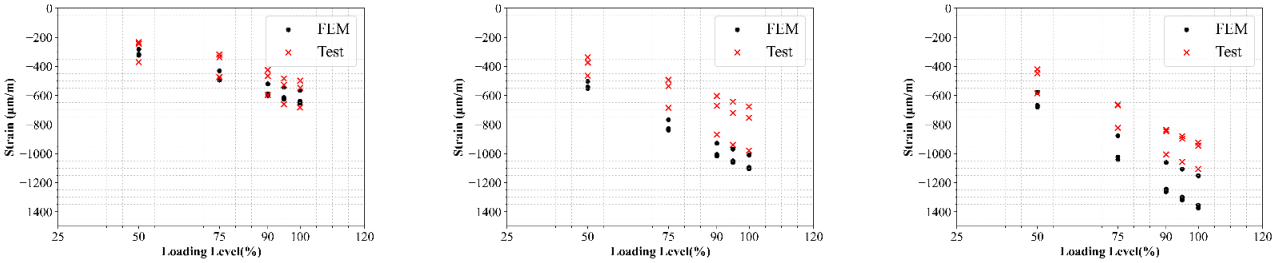

(a) Position S4 (b) Position S7 (c) Position S9

Fig. 11 Comparison of strain responses between the test and FEM results under C2 Broken (ASD)

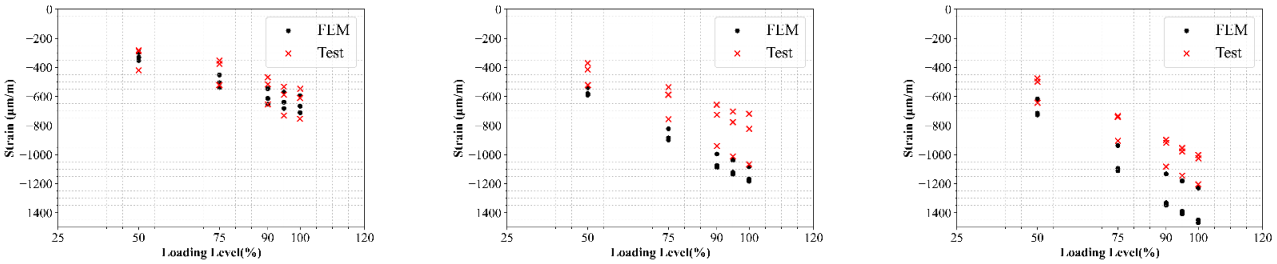

(a) Position S4 (b) Position S7 (c) Position S9

Fig. 12 Comparison of strain responses between the test and FEM results under C2 Broken (LRFD)

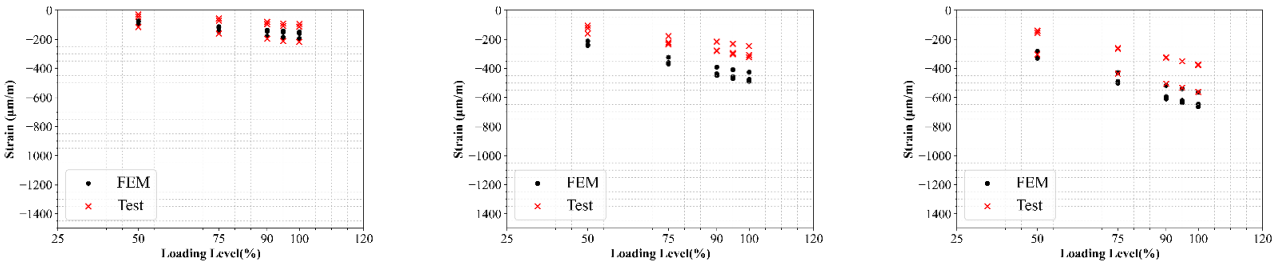

(a) Position S4 (b) Position S7 (c) Position S9

Fig. 13 Comparison of strain responses between the test and FEM results under One side not install (ASD)

Table 5 Loading sequence during full-scale test

Case No.	Type	Description	Method
1	Normal wind	Normal wind condition	LRFD
2	G.W. Broken	Broken ground wire (shield wire)	ASD
3	G.W. Broken		LRFD
4	CD2 Broken	Broken second wire	ASD
5	CD2 Broken		LRFD
6	One Side Not Installed	Conductors not installed on one entire side of the four arms	ASD
7	One Side Not Installed		LRFD
8	All wire intact (Low)	90 ° extreme wind with icing load	ASD
9	All wire intact (Low)		LRFD
10	All wire intact	90 ° extreme wind	LRFD

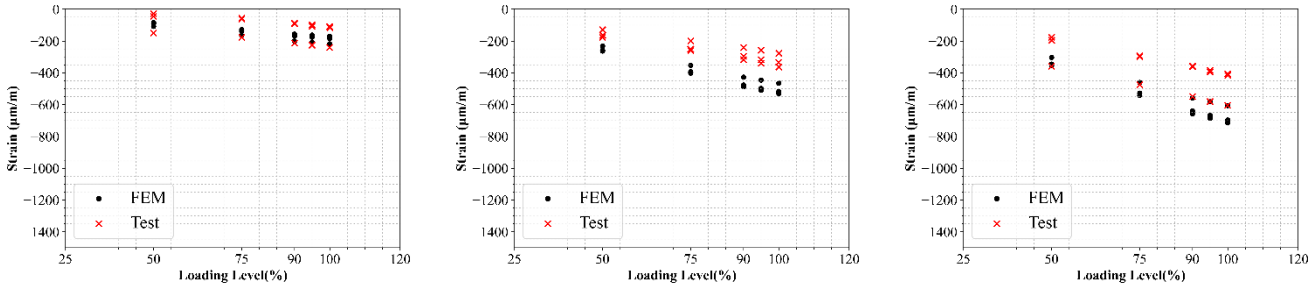

(a) Position S4 (b) Position S7 (c) Position S9

Fig. 14 Comparison of strain responses between the test and FEM results under One side not install (LRFD)

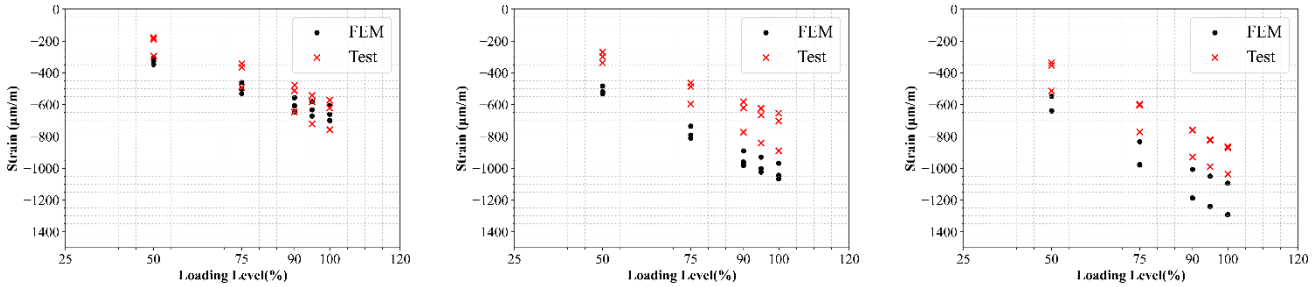

(a) Position S4 (b) Position S7 (c) Position S9

Fig. 15 Comparison of strain responses between the test and FEM results under All wire intact (Low) (ASD)

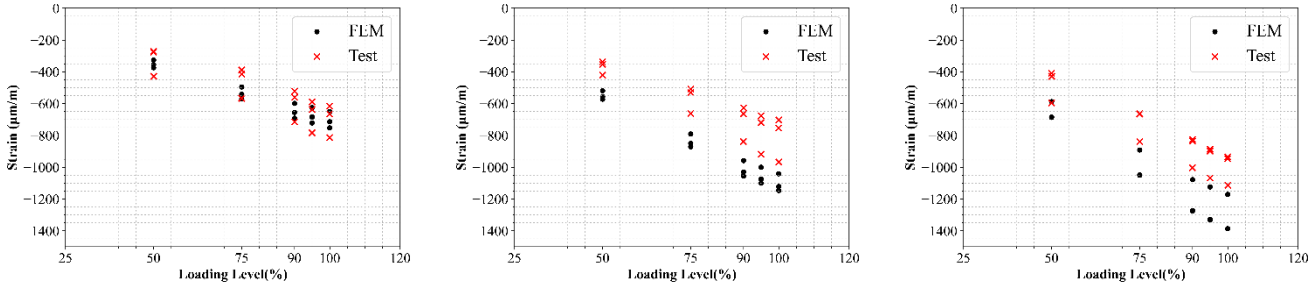

(a) Position S4 (b) Position S7 (c) Position S9

Fig. 16 Comparison of strain responses between the test and FEM results under All wire intact (Low) (LRFD)

seen at measurement points S7 and S9, the experimental strains were slightly lower than the FEM predictions, particularly for the lower structural members.

This discrepancy may be attributed to factors such as reduced effective member length owing to the physical joint size, assumed imperfections in the analysis, or stress redistribution to diagonal members. Nevertheless, all measured strains were within the range predicted by the

(a) Failure of tower overview

(b) Failure mode at s7

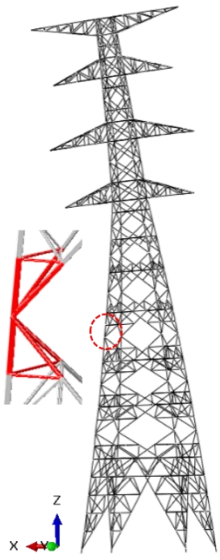

(c) Estimated failure at s7

Fig. 17 Ultimate failure of Transmission

FEM, indicating that the simulations provided a reliable representation of the actual structural behavior.

The strain values obtained under LRFD load conditions were consistently higher than those under ASD loads in both the FEM analysis and experimental results. Among all the evaluated load cases, the highest strain was observed at S9. In the FEM analysis, the greatest difference in strain between the ASD and LRFD loads occurred between Cases 2 and 3 with a maximum deviation of 8%, whereas the smallest difference of 6% was recorded between Cases 6 and 7. Similarly, in the experimental results, the maximum and minimum differences were observed in the same cases

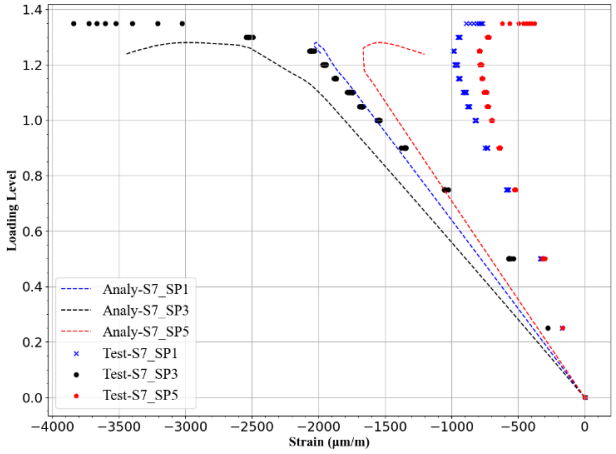

Fig. 18 Comparison of strain responses between FEM results and test at location S7 during failure test

with deviations of 9% and 7%, respectively, demonstrating a high level of consistency between the numerical and experimental findings.

As shown in Table 4, the wind load under the LRFD design method increased with structural height. This increased wind load resulted in higher lateral forces, which, in turn, amplified the axial forces and moments of the members. Consequently, both the FEM analysis and test results confirmed that the strain values were larger under the LRFD loads.

As previously mentioned, Cases 1–9 were conducted to evaluate the load-bearing capacity and structural integrity of the transmission tower by applying up to 100% of the test load. Across all the load cases, the member strains remained within the elastic range, thereby satisfying the load-bearing test requirements. Finally, a failure test of the structure was conducted under Case 10 loading conditions.

5.2 Failure test

A failure test of the transmission tower was conducted by applying Case 10 loading condition. Before initiating the test, strain gauges were used to confirm that no plastic deformation had occurred in the structural members, ensuring that the initial conditions were within the elastic range. A failure test was conducted by applying a factored design load in Case 10. The test began at a 0% load and progressively increased to 75%, 90%, and 100%, with each stage held for 1 min to assess structural stability. After verifying the structural load-bearing performance at 100% load, the load was incrementally increased by 5%, with each increment held for approximately 30 s to observe the member failure and deformation. The transmission tower ultimately failed owing to buckling failure at 130–135% of the design load. Fig. 17 shows the overall structural failure and failed members. The failure mode was identified as the buckling of the main members, which matched the initial failure location predicted by the FEM analysis.

Fig. 18 compares the strain values at the S7 member, where structural failure occurs. The strain values obtained from FEM analysis are represented as line graphs, whereas the experimentally measured strain values are shown as scatter points. The x-axis represents the strain and the y-axis indicates the Load Proportional Factor (LPF), which represents the ratio of the applied load to the design load. During the 130%–135% load stage, the member failed owing to buckling. During failure, a sudden increase in the transverse strain was observed at the vertex of the angle member owing to the buckling deformation, which exhibited the same trend as the nonlinear analysis results.

However, for points S1 and S5 located at the vertex of the angle sections, the overall trend was similar, but the experimentally measured strains were lower than those predicted by the FEM analysis. This discrepancy may indicate the influence of the bending moments on the stress istribution within the cross-section. Accordingly, it is more rational to consider both axial forces and bending moments in the structural design of members. Design formulations that account for the combined effects of the axial and bending actions may lead to more accurate and optimized outcomes.

Another key observation from the test results was the difference between the failure load ratio (1.35) observed in the experiment and the maximum LPF (1.25) obtained from the analysis. In the LRFD method, a compression member strength reduction factor of 0.9 is applied, accounting for various uncertainties such as material variability, construction errors, and imperfect modeling by serving as a safety factor. The ratio between the failure load in the test and the maximum load in the analysis was approximately 0.926, which closely aligned with the compression member strength reduction factor of 0.9, thereby demonstrating the validity of the applied design factor.

6. Conclusions

Building upon the growing need to transition from the traditional ASD to a more rational, strength-based approach, this study presents a comprehensive investigation into the structural behavior of a 345 kV lattice transmission tower designed using the LRFD methodology. Through nonlinear finite element analysis and full-scale testing, this study aimed to validate member strength equations and assess the accuracy of failure predictions. A comparative analysis between the LRFD- and ASD-designed towers under identical environmental conditions was performed, focusing on the dominant load scenarios. The key findings are summarized as follows.

• The conventional simplified design approach, which applies uniform wind pressure over the entire tower and evaluates member safety based solely on yield failure, fails to adequately capture structural vulnerabilities and failure behaviors. The strength-based LRFD approach, which incorporates the inelastic capacity beyond the elastic limit, was validated through analysis and experimental results to more precisely predict the failure mechanisms and ultimate load-carrying capacity of the transmission towers.

• Comparative testing under identical load conditions for both LRFD and ASD designs revealed similar trends between the nonlinear FEM analysis and experimentally

measured strain and failure modes. This confirms the necessity of incorporating geometric and material nonlinearities to accurately predict transmission tower failure behavior.

• Under the all-wire-intact loading condition, tower failure occurred through a sequence of partial yielding in the compression members, followed by a gradual increase in the ultimate load and ultimate buckling failure. This behavior is consistent with the FEM predictions.

• Although the LRFD loading condition produced higher strain values than the ASD condition, all observed strains remained within the yield limit. Specifically, the maximum measured strain under LRFD loads was under below 1,950 με, confirming elastic behavior even under increased axial and bending forces.

• Even with reduced member cross-sections based on the proposed design criteria, the transmission tower maintained structural safety under loading conditions designed using the conventional method. Furthermore, structural stability was confirmed under LRFD load combinations with applied load factors. The LRFD-designed tower ultimately failed at 135% of the factored design load, closely matching the 1.25 LPF predicted by nonlinear analysis, with less than 8% discrepancy between test and simulation.

• Overall, the LRFD approach achieved an 11.1% reduction in total tower weight, while ensuring safety margins consistent with analytical predictions. These results suggest that the proposed design criteria are reasonable and can be adopted.

Acknowledgments

This research was supported by a National Research Foundation of Korea (NRF) grant funded by the Korean government (MSIT) (RS-2021-NR060085).

References

AISC (2022), *Specification for Structural Steel Buildings, ANSI/AISC 360-22*, American Institute of Steel Construction, Chicago, IL, USA.

Deng, H., Li, F., Cai, Q., Dong, J. and Fu, P. (2017), "Experimental and numerical analysis on the slope change joint of a quartet-steel-tube-column transmission tower", *Thin-Wall. Struct.*, **119**, 572-585. https://doi.org/10.1016/j.tws.2017.07.006.

Deng, H.Z. and Huang, B. (2018), "Study on ultimate bearing capacity of main member in transmission tubular tower leg", *Thin-Wall. Struct.*, **127**, 51-61. https://doi.org/10.1016/j.tws.2018.01.025.

Fu, X., Wang, J., Li, H. N., Li, J.X. and Yang, L.D. (2019), "Full-scale test and its numerical simulation of a transmission tower under extreme wind loads", *J. Wind Eng. Ind. Aerod.*, **190**, 119-133. https://doi.org/10.1016/j.jweia.2019.04.011.

Gao, X., Yi, R., Zhang, L., Jiang, X. and Li, J. (2022), "Failure analysis of transmission tower in full-scale tests", *Buildings*, **12**(4), 389. https://doi.org/10.3390/buildings1204038.

Han, W.S., Kim, P., Kang, Y.J., Kim, S., Kim, J.H. and Kang, H. (2025), "Structural behavior and failure modes of 765kV transmission towers: A full-scale experimental study", *In IABSE Symposium: Environmentally Friendly Technologies and Structures: Focusing on Sustainable Approaches,* Tokyo, Japan, May.

IEC 60652 (2021), *Loading Tests on Overhead Line Structures*, International Electrotechnical Commission; Geneva, Switzerland.

Kim, J.M., Kim, S., Park, J.S. and Kang, Y.J. (2010), "Experimental study of steel transmission tower using partially scaled model", *J. Korean Soc. Steel Construct.*, **22**(4), 335-344.

Kim, P., Han, W.S., Kim, H., Kang, Y.J., Kim, S. and Kim, J.H. (2025g), "Analytical and Experimental Research on Transmission Towers with Simplified Design", *In IABSE Symposium: Environmentally Friendly Technologies and Structures: Focusing on Sustainable Approaches*, Tokyo, Japan. May.

Kim, P., Han, W.S., Kim, H., Kim, J.H., Kang, Y.J. and Kim, S. (2025b), "Experimental validation of a simplified structural design for transmission towers", *J. Construct. Steel Res.*, **226**, 109291. https://doi.org/10.1016/j.jcsr.2024.109291.

Kim, P., Han, W.S., Kim, H., Kim, J.H., Kang, Y.J. and Kim, S. (2025d), "Simplified design of power transmission tower: Strategic variable analysis study", *Structures*, **71**, 108084. https://doi.org/10.1016/j.istruc.2024.108084.

Kim, P., Han, W.S., Kim, H., Kim, J.H., Kang, Y.J. and Kim, S. (2025e), "Forensic investigation of unexpected failure in a full-scale transmission tower test", *Eng. Fail. Anal.*, **169**, 109175. https://doi.org/10.1016/j.engfailanal.2024.109175.

Kim, P., Han, W.S., Kim, H., Kim, J.H., Kang, Y.J. and Kim, S. (2025f), "Investigation of load-carrying capacity and failure mechanisms in full-scale testing of a re-fabricated transmission tower", *Eng. Fail. Anal.*, **171**, 109342. https://doi.org/10.1016/j.engfailanal.2025.109342.

Kim, P., Han, W.S., Kim, J.H., Kang, Y.J. and Kim, S. (2025a), "Rational arrangement of horizontal members for transmission towers considering the effects on the structural behaviors", KSCE *J. Civil Eng.*, **29**(6), 100143. https://doi.org/10.1016/j.kscej.2024.100143.

Kim, P., Han, W.S., Kim, J.H., Kang, Y.J. and Kim, S. (2025c), "Full-scale test of a lattice transmission tower designed by the LRFD-based standard", *Structures*, **77**, 109217. https://doi.org/10.1016/j.istruc.2025.109217.

Kim, P., Han, W.S., Kim, J.H., Lee, J., Kang, Y.J. and Kim, S. (2023), "Analytical investigation of the effects of secondary structural members on the structural behaviors of transmission towers", *Buildings*, **13**(1), 223. https://doi.org/10.3390/buildings13010223.

Korea Building Code (2016), *Korea Building Code and Commentary*, Architectural Institute of Korea; Seoul, Korea.

Korea Electric Power Corporation (2012), *Design Code of Electric Transmission Tower in Korea (DS-1111)*, Korea Electric Power Corporation (KEPCO); Seoul, Korea.

Kwon, K., Choi, Y., Choi, Y., Han, W.S., Kim, J.H. and Kong, J.S. (2024), "Extended limit-collapsed surfaces using fragility analysis of high voltage transmission towers located in coastal areas under wind load", *Adv. Struct. Eng.*, **27**(12), 2116-2132. https://doi.org/10.1177/13694332241263866.

Li, J.X., Zhang, X.H. and McClure, G. (2022), "Numerical and full-scale test case studies on post-elastic performance of transmission towers", *Engi. Struct.*, **259**, 114133. https://doi.org/10.1016/j.engstruct.2022.114133.

Li, Y., Li, Z., Yan, B. and Yan, Z. (2017), "Wind forces on circular steel tubular lattice structures with inclined leg members", *Eng. Struct.*, **153**, 254-263. https://doi.org/10.1016/j.engstruct.2017.10.032.

Ma, R., Yu, L., Zhang, H., Tan, L., Kueh, A.B., Feng, J. and Cai, J. (2021), "Experimental and numerical appraisal of steel joints integrated with single-and double-angles for transmission line towers", *Thin-Wall. Struct.*, **164**, 107833 https://doi.org/10.1016/j.tws.2021.107833.

Mohammadi Darestani, Y., Shafieezadeh, A. and Cha, K. (2019), "Effect of modelling complexities on extreme wind hazard performance of steel lattice transmission towers. Structure and Infrastructure", *Engineering*, **16**(6), 898-915. https://doi.org/10.1080/15732479.2019.1673783.

prEN 1993-1-14 (2023), *Eurocode 3 – Design of steel structures – Part 1-14: Design by FE Analysis*, European Committee for Standardization (CEN); Brussels, Belgium.

Rao, N.P., Knight, G.S., Mohan, S.J. and Lakshmanan, N. (2012), "Studies on failure of transmission line towers in testing", *Eng. Struct.*, **35**, 55-70. https://doi.org/10.1016/j.engstruct.2011.10.017.

Roman, R.R., Miguel, L.F.F. and Alminhana, F. (2024), "Model uncertainty applied to the failure analysis of transmission towers", *Eng. Fail. Anal,* **158**, 108023. https://doi.org/10.1016/j.engfailanal.2024.108023.

Song, C., Shafieezadeh, A. and Xiao, R. (2022), "High-dimensional reliability analysis with error-guided active-learning probabilistic support vector machine: Application to wind-reliability analysis of transmission towers", *J. Struct. Eng.*, **148**(5), 04022036. http://dx.doi.org/10.1061/(ASCE)ST.1943-541X.0003332.

Tian, L., Liu, J., Chen, C., Guo, L., Wang, M. and Wang, Z. (2020a), "Experimental and numerical analysis of a novel tubular joint for transmission tower", *J. Construct. Steel Res.*, **164**, 105780. https://doi.org/10.1016/j.jcsr.2019.105780.

Tian, L., Pan, H., Ma, R., Zhang, L. and Liu, Z. (2020b), "Full-scale test and numerical failure analysis of a latticed steel tubular transmission tower", *Eng. Struct.*, **208**, 109919. https://doi.org/10.1016/j.engstruct.2019.109919.

Tian, L., Yang, M., Liu, S., Liu, J., Gao, G. and Yang, Z. (2023), "Collapse failure analysis and fragility analysis of a transmission tower-line system subjected to the multidimensional ground motion of different input directions", *Structures*, **48**, 1018-1028. https://doi.org/10.1016/j.istruc.2023.02.042

Wang, J., Li, H. N., Fu, X. And Li, Q. (2021), "Geometric imperfections and ultimate capacity analysis of a steel lattice transmission tower", *J. Construct. Steel Res.*, **183**, 106734. https://doi.org/10.1016/j.jcsr.2021.106734.

Yu, Y., Paulino, G.H. and Luo, Y. (2011), "Finite particle method for progressive failure simulation of truss structures", *J. Struct. Eng.*, **137**(10), 1168-1181. https://doi.org/10.1061/(ASCE)ST.1943-541X.0000321.

Zhang, D., Hu, X., Song, X., Deng, H. and Ma, X. (2022), "Investigation on aerodynamic characteristics for steel tubular cross-arms of transmission tower under skew wind", *J. Wind Eng. Ind. Aerod.*, **222**, 104914. https://doi.org/10.1016/j.jweia.2022.104914.

Zheng, H.D., Fan, J. and Long, X.H. (2017), "Analysis of the seismic collapse of a high-rise power transmission tower structure", *J. Construct. Steel Res.*, **134**, 180-193. https://doi.org/10.1016/j.jcsr.2017.03.005.